This paper covers the detailed modeling we will require to produce PDF and PSD terrain profiles for C2M2L. For critical reviews, please mark up and send to paul.pukite@baesystems.com ... in process



# *Unified characterization of surface topography for vehicle dynamics applications*

**Abstract:** Environmental models by their nature contain a great deal of uncertainty. Since the underlying behavior of the model is rarely controlled by an ordered process, any model characteristics will carry along with it a level of aleatory uncertainty governed by the natural disorder. This paper applies novel uncertainty characterization approaches to classes of topographic models to demonstrate how to quantify the natural order and distinguish from artifical (man-made) order.

## Preface

Comprehensive vehicle testing requires *environmental context* models to evaluate a design's robustness and fitness for use. For a ground vehicle designed for both on-road and off-road use, interactions with the terrain provide an important testing context. For amphibious vehicles, the environmental context extends to sea states and aquatic currents. As an overriding factor, being able to traverse and navigate successfully various surface topographical features plays a large role in verifying that a vehicle's requirement specifications can be met.

To streamline the verification process, terrains need to be first well characterized and then modeled comprehensively enough that probability of correctness approaches can be applied. Without the ability to quantify for the probability of occurrence for a specific environmental effect, any requirements based on topography, such as traverse grade, can't be propagated to a virtual test of the vehicle's design ─ and thus we cannot substantiate with any degree of certainty or accuracy whether the vehicle meets the customer's needs.

## Primer on Characterization and Modeling

To develop some breadth, the models will cover both land and aquatic topographies. The landform aspects we refer to as *terrain modeling*[1] and the aquatic as *wave* (or *wave energy*) *modeling*.[2]

For terrains we consider a rigid model of altitudes as a function of lateral dimension. Often, a one-dimensional path, with provision for left and right tracks, is sufficient to characterize a terrain. The interaction of the vehicle with this type of terrain path provides enough of a context to virtually verify requirements such as absorbed power at speed and fuel efficiency on inclined grades.

*Stochastic models*[3] work very effectively to describe natural as well as artificial, man-made terrain. Enough disorder and randomness exists in the natural world, and even within an artificial world of cobblestones, chatter strips, and wave machines, that a synthetic model using probability concepts appears indistinguishable from an empirically measured set of real-world data.[4]

The stochastic tools of the trade include probability distribution functions, autocorrelation functions, power spectral densities, and moment distributions.[5]

*Probability density functions* (PDF) model sample spaces. A single PDF graph facilitates the characterization of natural phenomena that are prevalent in context modeling, including terrain slope distributions as well as wind, rainfall, lakes, cloud, etc.[6] Many of these models reduce to fairly simple analytical forms. For disordered systems and data containing aleatory uncertainty[7], we use techniques

such as the *maximum entropy principle*[8] and *super-statistics*[9], which have a more formal basis than heuristic models can provide[1]. For narrow distributions, we can apply Normal or Gaussian statistics.

*Autocorrelations* (ACF) and *power spectral densities* (PSD) are tied closely together. In basic terms, an autocorrelation describes the amount of similarity between two points separated spatially or temporally. For static terrain this is a purely spatial consideration, but at a constant vehicle speed, an autocorrelation turns into a temporal characteristic, as time equates to motion across a terrain. A PSD contains the same information as an ACF but works in the inverse space, either the wavenumber ($k$) space in the spatial domain, or frequency ($\omega$) space in the time domain. The decision to select an autocorrelation function or power spectral density will depend on the application. A spectral representation can easily provide reconstructed instances for either spatial or temporal domains in a general system context. The power of the real space autocorrelation is that it can recover a synthetic representation of the local terrain as a random walk model, while the PSD can approximate a varied terrain as a superposition of sine waves.

In addition, certain *multiscale* metrics[10] are useful to further characterize and in particular disambiguate potentially degenerate model descriptions. In particular, the multiscale entropy measure can be applied to temporal and spatial scales covering a wide dynamic range, and multiscale variances are sensitive to asymptotic behavior. What this tells us is the amount of disorder and uncertainty in the data, which is important as a concise supporting characterization metric.

*Table 1: Stochastic Model Categories*

| Stochastic Model | | Includes and Related | |
|---|---|---|---|
| Probability Density Function | PDF | Cumulative Distribution Function, Histogram | Position Independent |
| Autocorrelation Function | ACF | Correlation, Autocovariance | Relative |
| Power Spectral Density | PSD | Power Spectrum, Periodogram, Fourier Spectrum | Relative |
| Multiscale Analysis | MSA | Multiscale Variance, Multiscale Entropy | Relative |

**Table 1** above categorizes the stochastic models used to characterize terrain and waves. These can work together to model some sophisticated profiles. For example, a probability density function can model a length distribution, which then gets applied to a semi-Markov formulation for an autocorrelation analysis. By then applying a *Fourier transform* to the autocorrelation, we can arrive at a very concise representation. We will describe this in the analysis section.

## Data Characterization

The rules for construction of probability density functions follow from some elementary principles. Samples from experimental data are ranked, and then normalized to the largest (i.e. scarcest) sample. This establishes a cumulative probability of unity when integrated over the sampled data space. The rank histogram is then converted to a cumulative distribution function by interpolating across a continuum, and then a PDF derives from the first derivative with respect to the random variate. Strictly speaking, a PDF is a discrete (binned) form while a probability mass function (PMF) is the continuum, but we will go with the name PDF even though we assume the continuum.

Given that $X$ is some variate of interest, then a PDF described by $f(X)$ can be used to generate moments of the distribution, such as the expected value $\mathbf{E}[X]$.

$$\mathbf{E}[X] = \bar{X} = \int_{-\infty}^{\infty} X\, f(X)\, dX$$

[1] The sample size needed to reduce the variance of the statistics can be reduced by efficient applications of random sampling such as importance sampling.

Autocorrelation functions consider the pair-wise expected value of all samples separated by a distance measure. This describes the affinity for localized interactions that a PDF lacks sensitivity to. The computational complexity of calculating an autocorrelation can go as $N^2$, but a full computation is not always necessary for determining only closely separated distance correlations. Due to the *Wiener-Khinchin* theorem, the Fourier Transform of the data itself, calculated as a power spectrum of magnitude squared, is equal to the Fourier Transform of the autocorrelation, so that an inverse Fourier Transform of the directly calculated power spectrum will recover an autocorrelation. Due to the efficiency of a FFT, the computational time is order N×log(N), so this is often used to produce an ACF and a PSD with only frequency spectrum tools.

The power spectrum and autocorrelation are related by the following equation:

$$S_{xx}(f) = \int_{-\infty}^{\infty} r_{xx}(\tau) e^{-2\pi i f \tau} d\tau$$

Where the autocorrelation is defined as

$$r_{xx}(\tau) = \mathbf{E}\,[\, x(t) \cdot x^*(t-\tau)\,]$$

The double *xx* indicates that the expected value is between pairs of points along the terrain, with the τ serving as the sample-to-sample distance measure. (The asterisk indicates the complex conjugate, which does not apply for these signals.)

## Foundation of Stochastic Model Analysis

The analysis of real-world PDF's is aided by the fact that independence is assumed in the sample space. Each draw from a PDF is by definition independent and *stationary* with respect to the sampling point. We don't always have to understand and assert independence but enough empirical studies have been done to understand when the premise will work and when it doesn't.

For distributions based on energetic processes, the *principle of maximum entropy* often results in parsimonious fits to collected data (later will show extended examples for ocean and terrain). The selection of the variate is important, as the shape of the distribution can be thin-tailed (exponential or Normal distributed) or fat-tailed (a power-law) depending on its modeled derivation. For example, a timing distribution may be fat-tailed because the analyzed variate is velocity (which would ostensibly give a thin-tail) but since time appears in the denominator with respect to velocity, the eventual PDF generates much more weight in the tails.

For an ACF, the typical realization is via a random-walk model, often described by a *Markov* or *semi-Markov* process[11]. Higher order localized interactions beyond that, such as the near-neighbor memory-less Markovian random walk, can generate smoothed/filtered or ordered/periodic profiles, depending on the signs and strengths of the interactions. This has significance for decoding both an ACF and a PSD. An important consideration for autocorrelations is the concept of *coherence* length. A coherence length is that distance at which long-range correlations cease to factor in. Beyond that point, the state of the system could just as easily be determined by a draw from a PDF. This has significant implications on whether to apply a Fourier Transform or invert a PDF to analyze a power spectrum

The interplay between the use of PDF and ACF profiles for characterization is abetted by some very practical aspects of working in the spatial frequency domain. One novel way of looking at the problem derives from the world of diffraction spectroscopy, where because of the micro-scales involved, the only way possible to get insight is to immerse oneself in the inverse of the spatial domain, and into the spatial frequency domain, in what is known as *reciprocal space.*[12]

We will work in reciprocal space here, not because we can't detect the spatial features with measurements, but because the convenient mating of stochastic processes combined with powerful spectral algorithms, allows us to work out an analysis with greater rigor and statistical accuracy. This has huge implications for generating synthetic terrains based on limited real-world data.

## Unified Autocorrelation Analysis

The analysis based on characterizing stationary profiles. This is fully documented in a couple of heavily cited papers that derive the *pair correlation* (autocorrelation) functions of arbitrary surfaces. The derivation assumes a path in essentially a 2-dimensional slice. One dimension is the distance along the path of traversal and the other dimension is the elevation of the point along that path.

A surface is constructed with $N_c$ rigid cells arranged in the x- and z-directions. In a discrete approximation, the cell spacing in the x-direction is *a*, and in the z-direction is *d*. This surface is described by a function *f(x,* z) which is equal to 1 if there is a surface cell at coordinates *(x, z)* and 0 otherwise. The Fourier power spectrum is defined as:

$$I(\vec{S}) = \left| \sum_{\vec{r}} f(\vec{r}) e^{-i\vec{S}\cdot\vec{r}} \right|$$

Where $\vec{S}$ is the vector wavenumber defined in the reciprocal space of *(x, z)* as $(S_x, S_z)$. This can be rewritten as the equivalent Weiner-Khinchin relation:

$$I(\vec{S}) = N_c \left| \sum_{\vec{u}} C(\vec{u})\, e^{-i\vec{S}\cdot\vec{u}} \right|, \qquad N_c \to \infty$$

Where $\vec{u}$ is a real-space vector and

$$C(\vec{u}) = \frac{1}{N_c} \sum_{\vec{u}} f(\vec{r}) \cdot f(\vec{r} + \vec{u})$$

is the pair correlation function on the surface. It is the probability of finding two cells on the surface separated by a vector $\vec{u}$. By including the array of cells as a sum of delta functions, this equation can be changed to the integral form:

$$I(\vec{S}) = N_c \int_{-\infty}^{\infty} dx\, e^{-iS_x x} \sum_{l} e^{-iS_z ld} \left[ \sum_{n} \delta(x - na)\, C(x, ld) \right]$$

Where $C(x, ld)$ is the continuum portion of $C(\vec{u})$ written expressed along the two dimensions of interest. This can be rewritten making use of the *convolution theorem* as:

$$I(\vec{S}) = N_c \left[ \int_{-\infty}^{\infty} dx\, e^{-iS_x x}\, \delta(x - na) \right] \otimes \left[ \sum_{l} e^{-iS_z ld} \int_{-\infty}^{\infty} dx\, e^{-iS_x x} C(x, ld) \right]$$

Where $\otimes$ is the convolution operator, which expands the embedded summations. By taking the Fourier transform of the first term:

$$I(\vec{S}) = \left[\frac{2\pi N_c}{a}\sum_n \delta\left(S_x - \frac{2\pi n}{a}\right)\right] \otimes \left[\sum_l e^{-iS_z ld} \int_{-\infty}^{\infty} dx\, e^{-iS_x x} C(x, ld)\right]$$

This essentially says the second term repeats along the periodicity of the cell spacing, which is the result of a discrete representation. The second term is what we are interested in for a continuous system.

Let's next expand on the pair correlation term $C(x, ld)$. We first consider a surface in which the surface cells are allowed to be on any of an infinite number of levels as illustrated below. (Note that infinite specifically applies to the number of levels; for finite level systems, only the x-distance is infinite.)

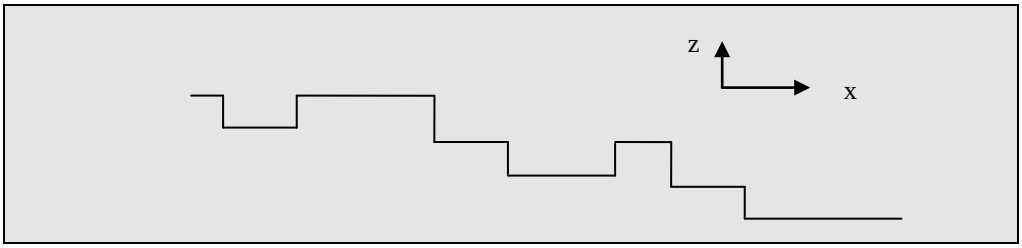


*Figure 1: A surface composed of terraces separated by levels*

The probability of finding a cell at the origin and at a position $(x, ld)$ away is the sum of the probabilities of all possible configurations of steps that separate these two points. For example, assume for the moment that all steps are same height and are always in the same direction as in the classic descending stair. And suppose that a sequence of levels with lengths $(L_1, L_2, \ldots, L_n)$ separate a cell at an origin that is $L_0$ away from the first step from a cell at $(x, ld)$ which is $L_n$ away from the last step. Then the probability of this configuration is

$$P_0(L_0)\, P_1(L_1) \cdots P_{n-1}(L_{n-1})\, P_n(L_n)\, \Delta L_0\, \Delta L_1 \cdots \Delta L_{n-1} \Delta L_n$$

Where the $P_i(L_i)$ with i = 1, 2, . . . , $n$ -1 are the probabilities per unit length of a terrace of length $L_i$ occurring on the $i^{th}$ level of the surface. The function $P_0(L_0)$ is the probability per unit length that there is a cell at the origin that is $L_0$ before the first step. The function $P_i(L_i)$ is the probability that there is a cell $L_n$ away from the last step. The middle $n$ - 1 $P_i(L_i)$ are identical and equal to $P(L_i)$ for the infinite surface. This equation implicitly assumes that the "terrace" lengths are statistically independent from one another. The length of one does not determine the length of subsequent terraces except in so far as the sum of the $L_i$ equals the total x-coordinate and that the number of steps is $I$, which is equal to $n$ for the strictly descending staircase. To determine the pair correlation function, one must integrate over all possible configurations of steps that satisfy these constraints.

If in addition, we allow the step heights to be any multiple of the level separation, either positive or negative, with probability distribution $H(h_i)$ for a step of height $h_i d$, then the correlation function $C(x, ld)$ is

$$C^{+}(x, ld) = N_l \Bigg\{ P_{0f}(x)\delta_{l,0} + \sum_{n=1}^{\infty}\sum_{h_i=}^{\infty}\cdots\sum_{-\infty}^{\infty}\int_{L_i=}^{\infty}\cdots\int_{0}^{\infty} P_0(L_0)\times H(h_1)\,P(L_1)\cdots P(L_{n-1})H(h_n)P_f(L_n) \times\left[\delta\left(x-\sum_{i=0}^{n}L_i\right)\delta\left(x-\sum_{i=1}^{n}h_i\right)\,dL_0\,\cdots dL_n\right]\Bigg\}$$

This formulation is equivalent to a convolution integral of all the possible configurations of steps. The right hand side of this equation integrates over all possible configurations of terrace lengths, $L_i$, and sums over all possible step heights, $h_i$ *d* , that will add to give a displacement *(x, ld)* from the origin. The plus sign in the superscript indicates the correlation function for the positive *x* and *z*-directions; to obtain the negative directions, simply replace *x* by *–x* and *z* by *–z*. $N_l$ is the total number of levels involved and is required to approach infinity. The function $P_{0f}(x)$ is the probability that there is a cell at the origin and one *x* away on the same terrace with no jumps in between.

The two distribution functions *H( h)* and *P( L)* are normalized according to

$$1 = \sum_{h=-\infty}^{\infty} H(h). \qquad 1 = \int_{\tau=L}^{\infty} P(\tau)d\tau$$

The functions $P_0(L)$ and $P_f(L)$ can be written in terms of the terrace length distribution function *P(L)*. $P_0(L)$ is the probability that there is a cell at the origin and the first step is *L* away. It is given by the product of the probability that there is a cell at the origin, which is given by the coverage Θ, and the number of configurations that allow the first step to be at *L*. For the infinite staircase, the coverage is $1/N_l$ and

$$P(L) = \frac{\theta}{\langle L\rangle}\int_{\tau=L}^{\infty} P(\tau)d\tau$$

Where

$$\langle L\rangle = \int_{\tau=L}^{\infty} \tau\, P(\tau)d\tau$$

To find $P_f(L)$ it is important to realize the asymmetry of the method. Since the probability of being at step *n* is 1 by construction, $P_f(L)$ is simply given by the probability that the step is followed by a terrace of length $\tau > L$. Thus it is given as

$$P_f(L) = \int_{\tau=L}^{\infty} P(\tau)d\tau$$

For the important case of no level changes, or the $n = 0$ portion of the summation, $P_0(L_0)$ and $P_f(L_n)$ must be replaced by

$$P_{0f}(L) = \frac{\theta}{\langle L\rangle}\int_{\tau=x}^{\infty} (\tau - x)P(\tau)d\tau$$

as this is the correlation function of a single level. Similar derivations of the preceding probabilities applied to a microscopic domain can be found in [13].

To calculate the PSD, we want the Fourier transform of the correlation function for $C^{+}(x, ld)$ For this, first substitute the delta function representations

$$\delta\left(x-\sum_{i=0}^{n} L_i\right)=\frac{1}{2\pi}\int_{-\infty}^{\infty} dS_x\, e^{-iS_x\left(x-\sum_{i=0}^{n} L_i\right)}$$

$$\delta\left(l-\sum_{i=0}^{n} h_i\right)=\frac{1}{2\pi}\int_{-\infty}^{\infty} dS_z\, e^{-iS_z\left(l-\sum_{i=0}^{n} h_i\right)d}$$

into the long equation and define $P(S_x)$ and $H(S_z)$ by

$$P(S_x)=\int_{0}^{\infty} P(L)e^{-iS_xL}$$

$$H(S_z)=\sum_{-\infty}^{\infty} H(h)e^{-iS_zhd}$$

to be the Fourier transforms of the individual probability density functions. Also, the Fourier transforms of the other probability functions can be written in terms of $P(S_x)$ according to

$$P_0(S_x)=\frac{\theta}{iS_x\langle L\rangle}[1-P(S_x)]$$

$$P_f(S_x)=\frac{1}{iS_x}[1-P(S_x)]$$

$$P_{0f}(S_x)=\frac{\theta}{{S_x}^2\langle L\rangle}[1-P(S_x)]+\frac{\theta}{iS_x}$$

Then the correlation function becomes

$$C^{+}(x,ld)=N_l\left\{P_{0f}(x)\delta_{l,0}+\frac{1}{4\pi^2}\sum_{n=1}^{\infty}\left[\int_{-\infty}^{\infty} dS_z e^{-iS_zld}[H(S)]^n\right]\times\left[\int_{-\infty}^{\infty} dS_x\, e^{-iS_xx}P(S_x)\big(P(S_x)\big)^{n-1}P(S_x)\right]\right\}$$

Taking the transform to generate a PSD, we obtain:

$$I_0(S_x,S_z)=2\,N_l\,\mathrm{Re}\left\{P_{0f}(S_x)+\sum_{n=1}^{\infty}[H(S_z)]^nP_0(S_x)[P(S_x)]^{n-1}P_f(S_x)\right\}$$

Here, the subscript 0 on the power spectrum intensity indicates the Fourier transform of the continuum part of the correlation function. Calculating the geometric sum, the result is

$$I_0(S_x,S_z)=2\,N_l\,\mathrm{Re}\left\{P_{0f}(S_x)+H(S_z)\,P_0(S_x)P_f(S_x)\sum_{n=0}^{\infty}[H(S_z)P(S_x)]^n\right\}$$

$$=2\,N_l\,\mathrm{Re}\left\{P_{0f}(S_x)+\frac{H(S_z)\,P_0(S_x)P_f(S_x)}{1-H(S_z)P(S_x)}\right\}$$

$$=\frac{2\,N_l}{{S_x}^2\langle L\rangle}\,\mathrm{Re}\left\{1-P(S_x)-\frac{H(S_z)\,(1-P(S_x))^2}{1-H(S_z)P(S_x)}\right\} \qquad \textbf{(1)}$$

One simple realization of a surface forms a staircase of steps. Each step descends or ascends in one direction.. For this case, the transform of the step height distribution function, $H(S_z)$, becomes $e^{-iS_z d}$. We also assume that the staircase is not perfectly regular so that the sum in the equation always converges.

$$I_0(S_x, S_z) = \frac{2}{{S_x}^2\langle L\rangle} \frac{1 - |P(S_x)|^2}{|1 - P(S_x)e^{-iS_z d}|^2} \quad \textbf{(2)}$$

If we then flatten the staircase, this emulates a sawtooth pattern of topography, either a set of breaking waves or a graded terrain with that structure. To level the reciprocal space, all we need to do is follow a path along the equality $x+z/\theta$, as shown in the figure below. This maps the average terrain slope onto an affine transformed coordinate system that is flat from the perspective of the viewer. In reciprocal coordinates, the transformed path is $S_x + S_z\,\theta$

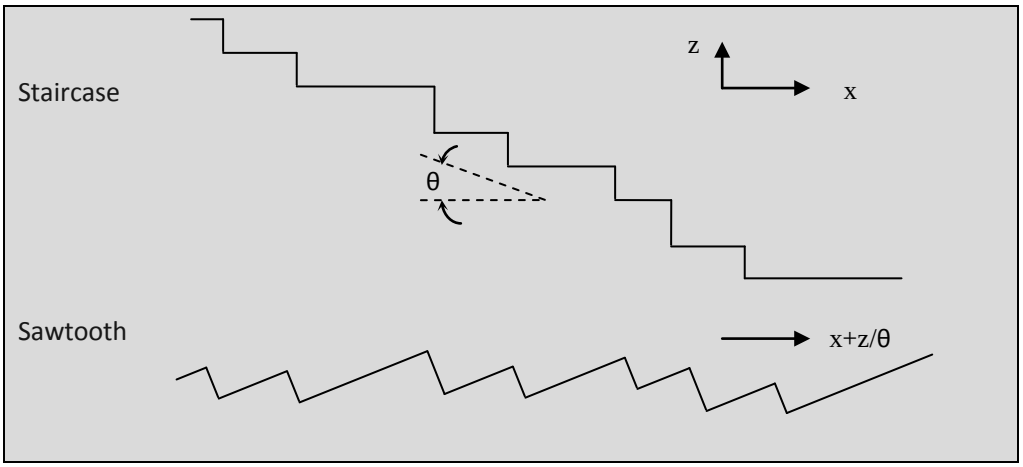


*Figure 2: A descending staircase is used to derive an autocorrelation and then the coordinate system is rotated to model a sawtooth terrain profile.*

The general approach falls under the categorization of a semi-Markov analysis. We allow the distribution for $P(S_x)$ and $H(S_z)$ to take on any form. To recover the elementary Markov spectrum, we apply a maximally disordered distribution to $P(L)$.

$$P(L) = \frac{1}{\langle L\rangle}\, e^{-L/\langle L\rangle}$$

This results in the Fourier transform for $P(S_x)$

$$P(S_x) = \frac{1}{1 + iS_x\langle L\rangle} \quad \textbf{(3)}$$

Applying the same transform to the step height, the resulting PSD is the Cauchy or Lorentzian profile:

$$I_0(S_x) = \frac{1}{4 + \langle L\rangle {S_x}^2} \quad \textbf{(4)}$$

This has the classic PSD second-order power-law fall-off of a random terrain, shown below. The deviations from this fall-off are due either to further order in the terrain relief or filtering of the data set. This particular data was extracted from an unclassified military test course.

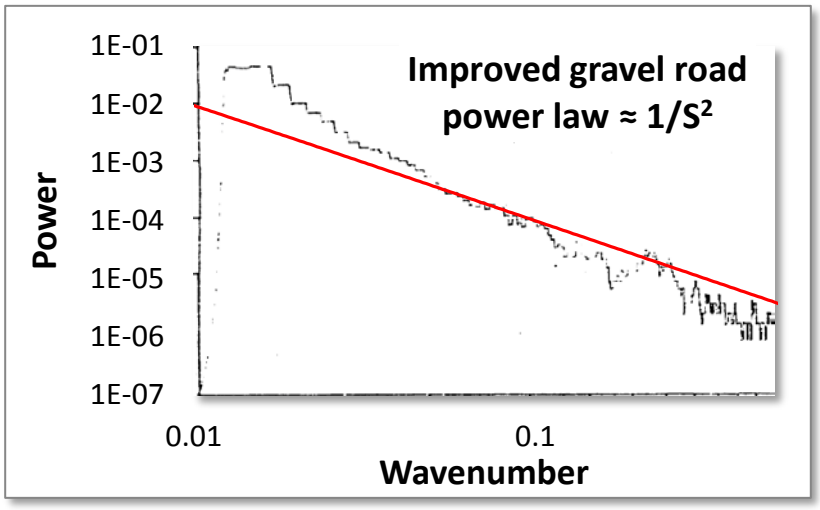


*Figure 3: Power Spectral Density (PSD) plot from a declassified military test course, with a random walk terrain profile overlaid as $1/S^2$*

The data and spectra from Figure 3 was taken from a historical unclassified test document. The following is the present day "rough road" test track data from a Mercedes-Benz course[14], note the reduced fluctuation noise and wide dynamic range in the data:

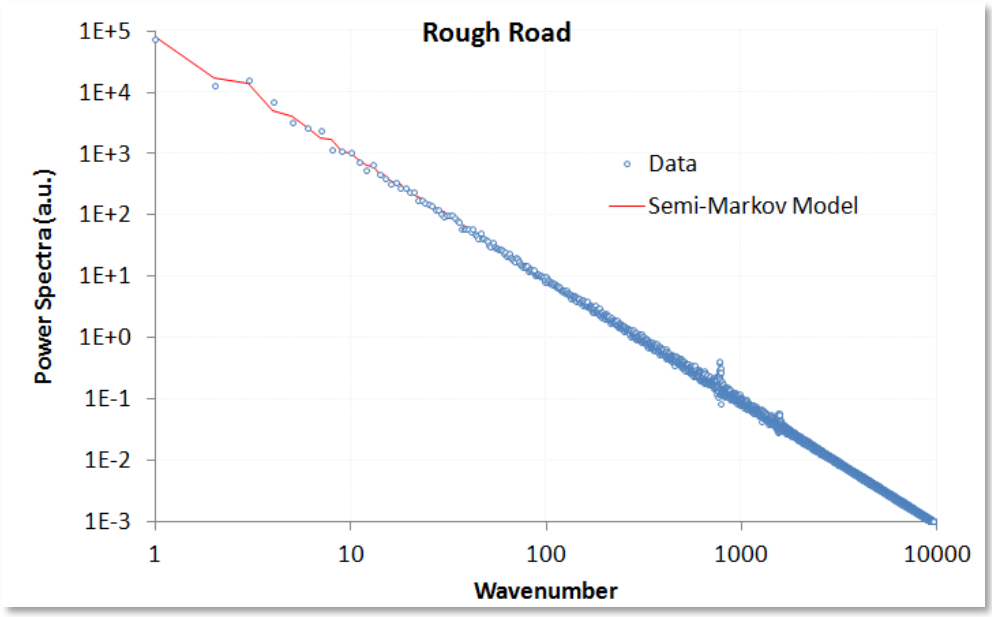


*Figure 4: PSD of data collected from a higher resolution and more extensive terrain data set from a Mercedes-Benz test track. Note the weak high frequency spike with a definite even harmonic signal. The overall tendency of the terrain profile follows a random semi-Markov model very well.*

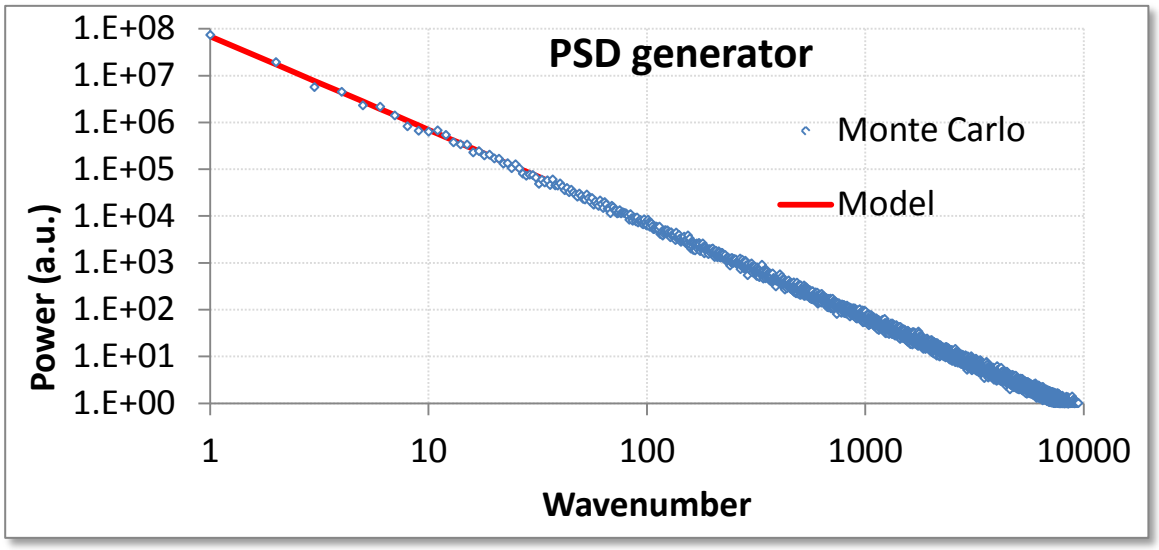


*Figure 5: Monte Carlo generated course based on random walk model*

The power of the analysis is that it can detect asymmetries in the surface relief. For example, a terrain that shows sawtooth waves will contain even harmonics (note the weak harmonic in Figure 4), while a terrain that contains symmetric square or rolling pseudo-sinusoidal waves will contain odd harmonics. Additionally, for the surface shown above, much detail may be obscured by a long-wavelength trend in the underlying terrain. The slope for the "rough road" example of Figure 4 is fairly large and this contributes to a strong $1/S^2$ tail above a certain wavenumber, i.e. a linear slope in real space generates a inverse squared response in reciprocal space according to Fourier analysis. This can also be inferred by the reduction of noise at high wavenumbers, since a static slope is deterministic and dominates over the stochastic fluctuations.

This all comes out of Fourier series decomposition of periodic waveforms, but here we apply it to stochastically varying waveforms – stochastic profiles are very prevalent in artificial and natural terrain, as we will describe next.

In the following sections, we will look more closely at the spectra features of aquatic and land terrain.

# Application to Aquatic Waves

We start with aquatic wave spectra because these have a more consistent character than land terrain. Gravity plays a critical role as it automatically detrends the data to maintain a level profile over the distances of interest. Sea waves also are very sensitive to long-range *coherence*, that is, the ability to maintain phase relationships over a significant distance.[15]

### Incoherent Wave Spectra

In the wild, waves display little coherence over long spatial scales. In other words, the knowledge that one wave has over another wave separated by several undulations is limited.

We make a maximum entropy estimation of the energy of a one-dimensional propagating wave driven by a prevailing wind direction. The mean energy of the wave is related to the wave height by the square of the height, **H**.[16] This makes sense because a taller wave needs a broader base to support that height, leading to a scaled pseudo-triangular shape, as shown in the figure below.

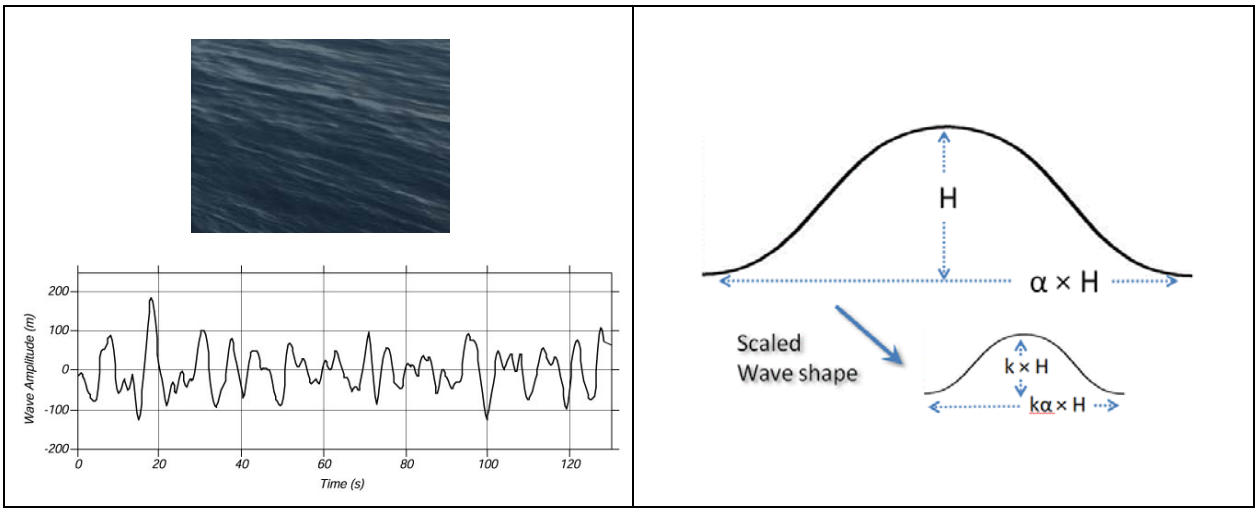


*Figure 6: (left) The goal is to model the spectral density of waves. Enough disorder exists in open water that periodic coherence between spatially separate waves is not maintained, measurement from wave buoy in north Atantic.* [17] *(right) The initial assumption is that waves contain energy proportional to their width and height. This proportionality scales independent of volume. Total energy in a directed wave goes as the square of the height, and the macroscopic fluid properties suggest that it scales to size. This leads to a dispersive form for the wave size distribution.*

Since the area of such a scaled triangle goes as $\mathbf{H}^2$, the MaxEnt cumulative probability is:

$$P(H) = e^{-aH^2}$$

where *a* is related to the mean energy of an ensemble of waves. This relationship is empirically observed from measurements of ocean wave heights over a sufficient time period. However, we can proceed further and try to derive the dispersion results of wave frequency, which is the very common oceanography measure. So we consider -- based on the energy stored in a specific wave -- the time, *t*, it will take to drop a height, *H*, by the Newton's law relation:

$$t^2 \sim H$$

and since *t* goes as 1/*f*, then we can create a new PDF from the height cumulative as follows:

$$p(f)df = \frac{dP(H)}{dH}\frac{dH}{df}df$$

where[18]

$$H \sim \frac{1}{f^2}$$

$$\frac{dH}{df} \sim -\frac{1}{f^3}$$

then

$$p(f) \sim \frac{1}{f^5} e^{-c/f^4} \quad \textbf{(5)}$$

which is just the Pierson-Moskowitz wave spectra that oceanographers have observed for years (developed first in 1964, variations of this include the JONSWAP, Bretschneider and ITTC wave spectra).

This concise derivation works well despite not applying the correct path of calculating an auto-correlation from ***p*(*f*)** and then deriving a power spectrum from the Fourier Transform of ***p*(*f*)**. As smooth ocean waves approach a sinusoidal ideal, a single wave will contribute a Fourier component at that frequency alone and the spectrum can be evaluated almost by inspection. This convenient shortcut remains useful in understanding the simple physics and probabilities involved.

As we have an interest in using this derived form for an actual potential application, we can seek out public-access stations to obtain and evaluate some real data[19]. The following data is extracted from the first region accessed — a pair of measuring stations located off the coast of San Diego[20].

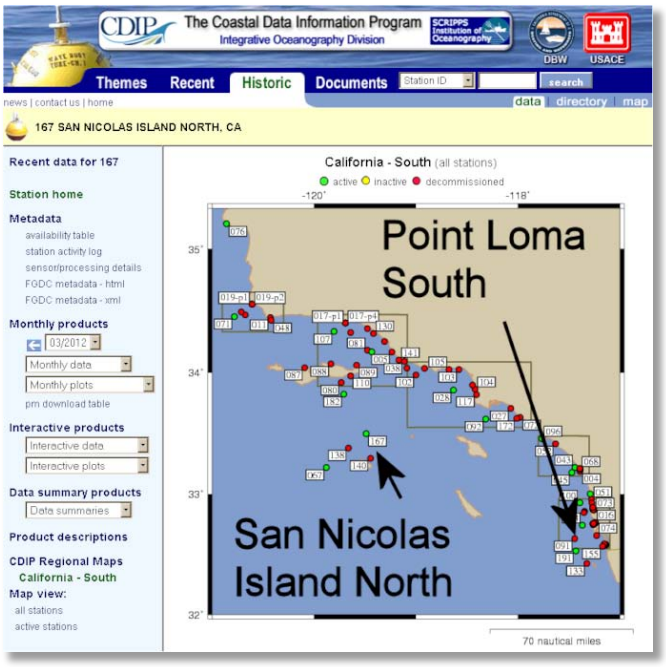


*Figure 7: The CDIP data source provided archival wave energy statistics to compare models against.*

The default data selector picked the first day of this year, 1/1/2012 and the station server provided averaged wave spectra for the entire day. The red points in Figure 8 below correspond to best fits from the derived MaxEnt algorithm to the blue data set. [2]

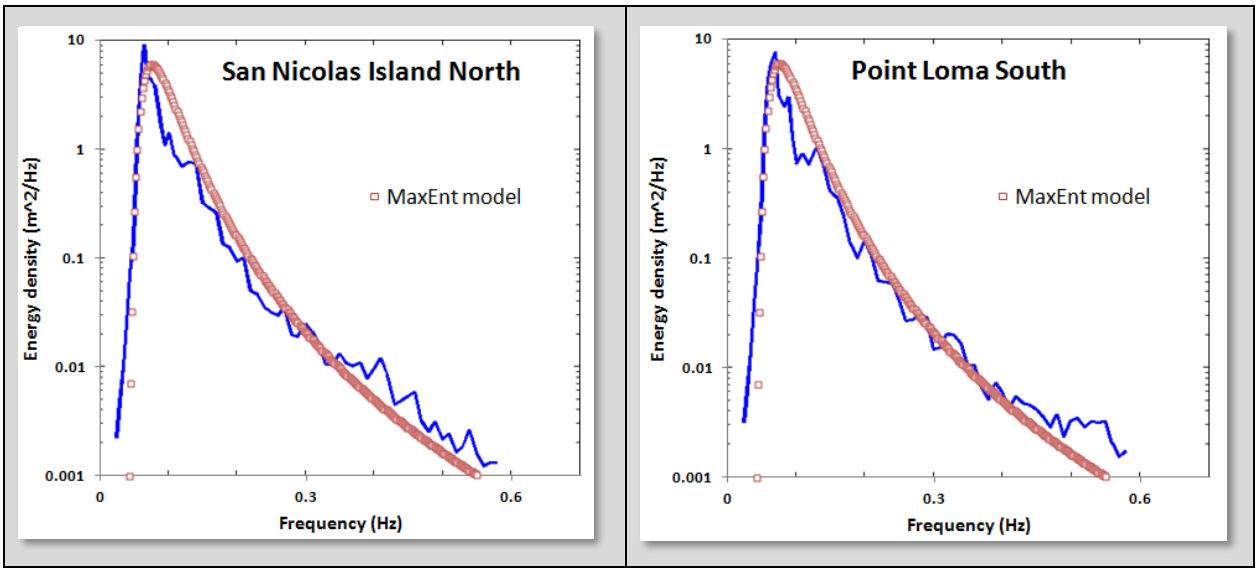


*Figure 8: Wave energy spectra from two sites off of the San Diego coastal region. The Maximum Entropy estimate is in red.*

Like many similar spectra such as wind and EMI, the wave spectrum derives simply from maximum entropy conditions.

Note that we did not need to invoke the spectral model presented earlier in this paper. The correlations are short over the sinusoidal shape of an individual wave and so those frequency components show up strongly in the energy density PSD. The implications are that the driving forcing function needed to provide order in the case of natural waves is missing, and this makes sense as main stimulus, wind energy, on its own is highly disordered. The wind simply stimulates the wave to maximize its entropy subject to the kinetic and potential energy that are provided.

On the other hand, under controlled conditions, more order can be supplied to make the waves appear more coherent over a spatial distance.

### Coherent Wave Spectra

Coherent waves are easier to generate in the laboratory than in the wild. A large wave tank, with waves generated by a consistent wind will clearly expose any ordered features in the PSD.[21]

In Figure 9 below, taken from [22], the measured PSD clearly shows clear harmonic peaks strongly suggestive of longer-range order in the wave periodicities. Superimposed on the data profile (shown in black) is a model adapted from the derivation of the previous section of this paper. Note that the time-domain frequency scale with the spatial-domain frequencies, as short, choppy waves have much smaller periods or cycle-times than the large, rolling waves. This means that we can apply a spatial analysis to the temporal analysis with some generality.

[2] To explore the dataset, here is a link to the interactive page : http://cdip.ucsd.edu/?nav=historic&sub=data&units=metric&tz=UTC&pub=public&map_stati=1,2,3&stn=167&stream=p1&xyrmo=201201&xitem=product25

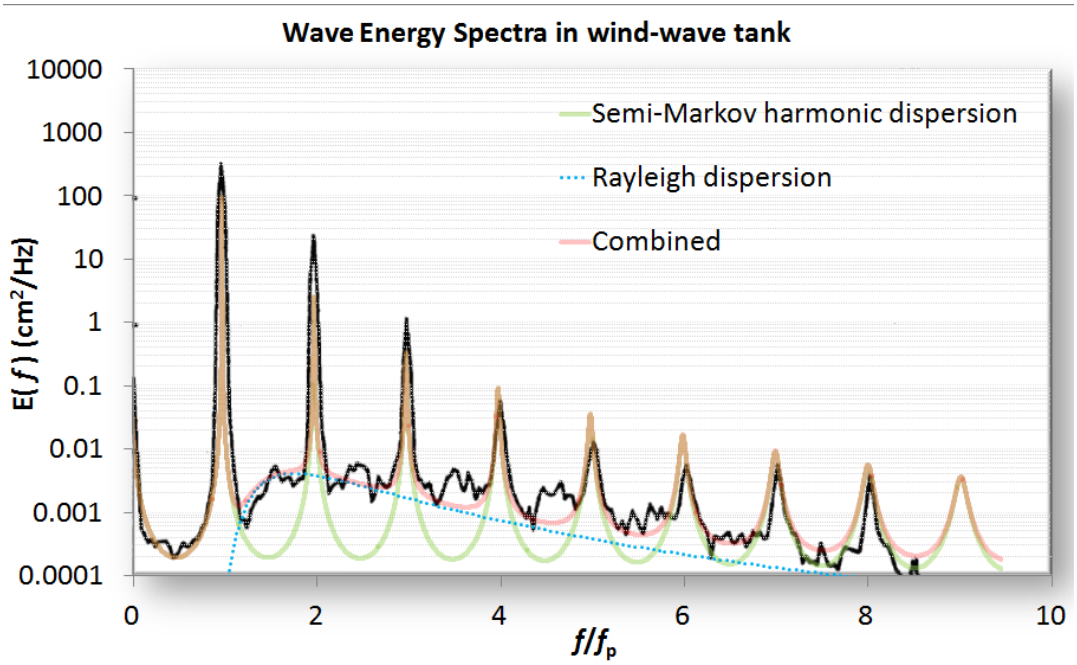


*Figure 9: Highly ordered waves with all harmonics generated in a wave tank*

The basic model is to choose a $P(L)$ wave density such that it reproduces the spacing and envelope of the harmonics. One of the simplest density functions is known as the shifted exponential. This maintains a minimum spacing with the possibility of an occasional longer wavelength:

$$P(L) = \begin{cases} 0, & L < L_0 \\ e^{-\alpha(L-L_0)}, & L > L_0 \end{cases} \quad \textbf{(6)}$$

This generates a Fourier transform

$$P(S_x) = \frac{e^{-iS_xL_0}}{1 + {iS_x}/{\alpha}}$$

And then the full power spectrum assuming a coherent relationship exists (see **Equation 1**):

$$I(S_x) = \frac{1}{(S_x - \alpha \sin(S_xL_0))^2 + \alpha^2(1 + \cos(S_xL_0))^2} \quad \textbf{(7)}$$

$$I(S_x) = \frac{1}{(S_x + \alpha \sin(2S_xL_0))^2 + \alpha^2(1 - \cos(2S_xL_0))^2} - \frac{1}{S_x{}^2(1 + \alpha L_0)^2} \quad \textbf{(8)}$$

These two formulations, scaled accordingly, generate the semi-Markov harmonic dispersion model shown in Figure 9. The first equation generates an odd-harmonic waveform due to a symmetric view of up and down steps. The latter equation assumes an all-harmonic composition derived by assuming a surface with a saw-tooth set of steps, which is likely nearer the real situation for stimulated waves.

Note that as $L_0$ approaches zero, then the Markov random walk is recovered (see equation **4**). Thus a simple parametric model with the two coefficients related by a *characteristic period*, $< L >$, can emulate the continuum of order to disorder:

$$\langle L \rangle = L_0 + 1/\alpha$$

As $L_0$ approaches $< L >$ the spectrum will show strong harmonics. As $L_0$ approaches 0, the random aspect will suppress the harmonics. As an example of this continuum consider Figure 10 below:[23]

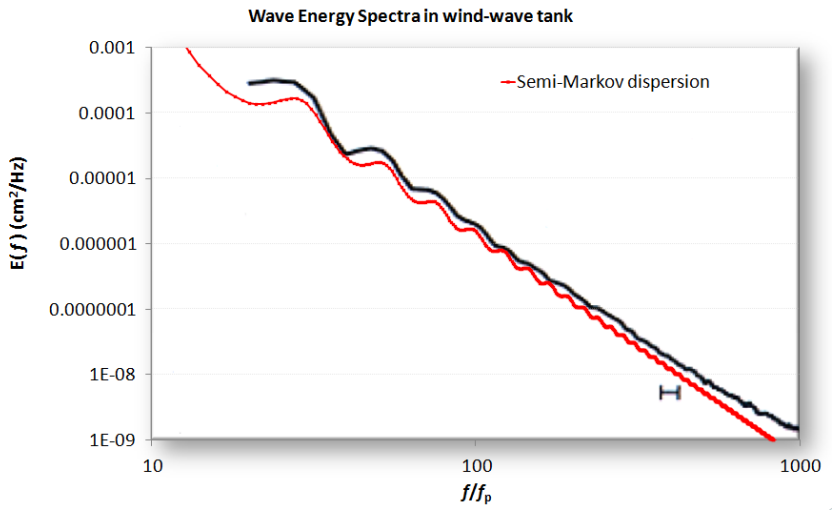


*Figure 10: A PSD from a wave tank showing ripples*

Note that the dispersion model does, by definition, generate square or sharp edges. Unless there are breakers in the waves, the actual profiles will get rounded. By applying a low-pass filter to the model, the actual waveform will reveal reduced high frequency components and give better agreement with the spectral data. Another example, fit from a simulated wave[24] is shown below:

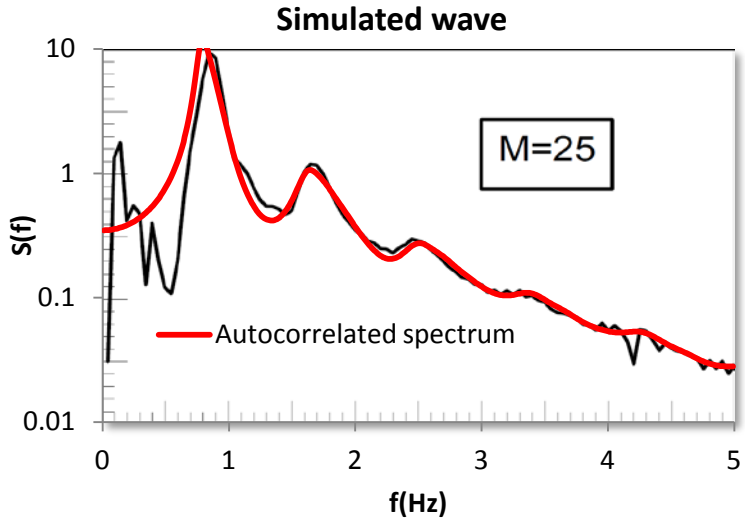


*Figure 11: A simulated wave which emulates crest-focused dynamics shows intermediate order*

In general, aquatic wave coherence showing strong harmonics occurs under more controlled conditions than normally exist in the wild.

# Application to Landforms and Terrain

For terrains we use the same approach as for wave spectra. The significant geometric scale distinction between terrain profiles and aquatic wave profiles is that the former can have very long range variations, stretching to the scale of mountain ranges.

### Incoherent Terrain Correlations

Statistics over an extensive large-scale terrain database provides the best example of incoherent variations in surface topography. Figure 11 derives from a detailed terrain slope case study reported in [25]. The derivation assumed that maximally sloped regions had larger potential energy and a maximum entropy (MaxEnt) statistical distribution would follow. The chart in Figure 11 is from a single region and that of Figure 12 from the entire country. The former follows an exponential and the super-statistical latter follows a Bessel distribution.

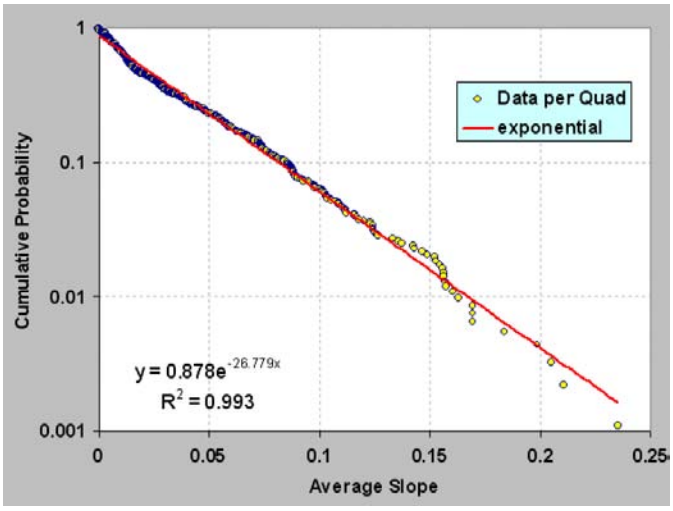


*Figure 12 : Probability density function of terrain slopes for an isolated region*

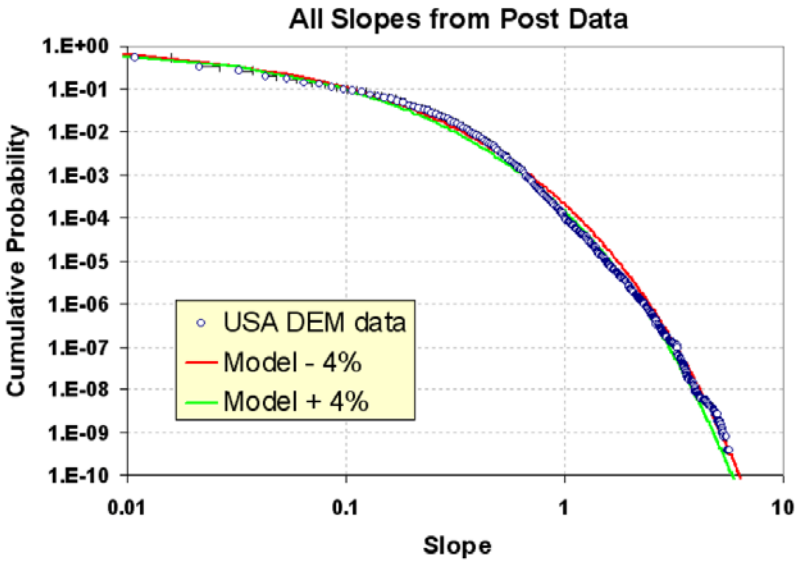

*Figure 13 : Probability density function for a wide area*

### Coherent Terrain Spectra

Coherent terrain spectra exist on a much shorter scale. The objective is to model the fine terrain, both random roughness as described in Figure 4, and more periodic features such as cobblestones[26] and washboard[27] as shown in Figure 13 below:[28]

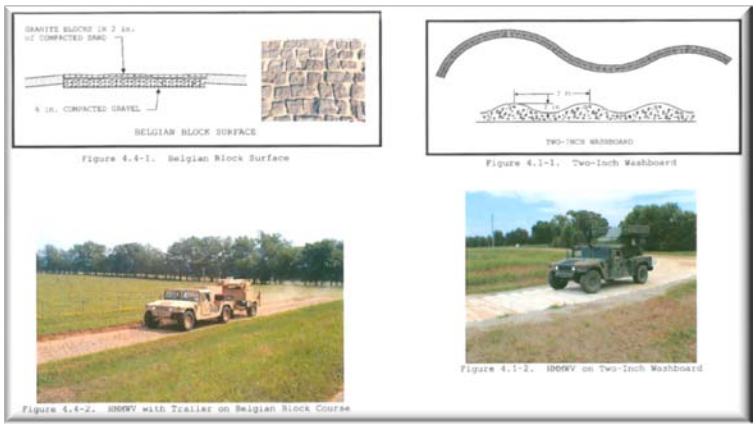


*Figure 14: (left) Cobblestone test track and (right) Washboard test track*

Mercedes-Benz test track data used in Figure 4 was also applied to a particular style of road cobblestone paving known as *Belgian Block*. This data was supplied in *OpenCRG* format,[29] and covered the track shown in the Google Earth snapshot shown below in Figure 14


*Figure 15: The OpenCRG terrain format features a header which indicates the geospatial location of the data set. This winding Belgian Block course was located underneath an overpass on the Mercedes-Benz campus in Stuttgart, with the start of the path indicated by the green arrow.*

A typical one-dimensional profile trace is shown below in Figure 15. Clearly visible are two levels of terrain variability. One variation on the order of 10 cm height contributes to swales on the test track and the other, a fine-grained roughness on the order of 1 cm, are caused by the cobblestone blocks themselves.

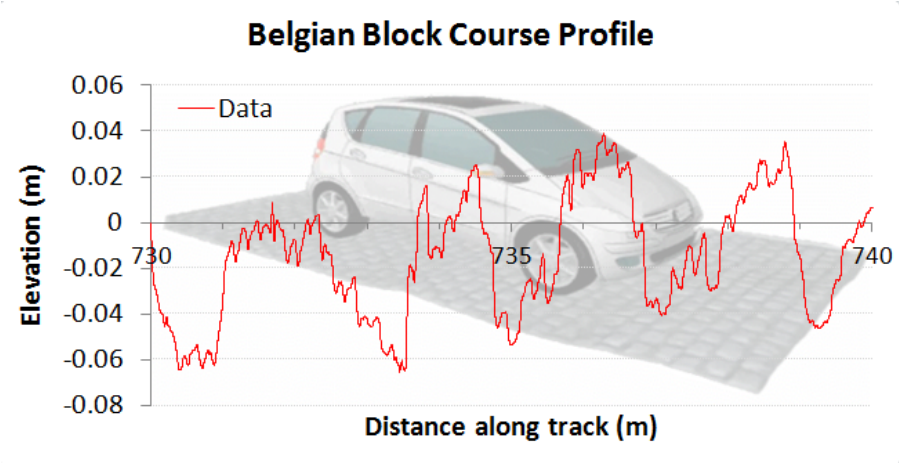


*Figure 16: A profile trace along a short path of the test track indicates the roughness.*

The fine resolution of the data is shown in Figure 16, which is on the order of 1 cm in the lateral dimension.

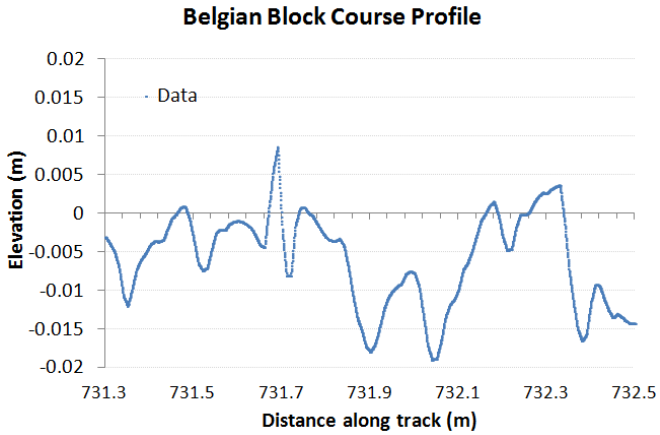


*Figure 17 : A very short profile along the test track showing the Belgian Block variability.*

The PSD calculated for this course is shown in Figure 17. Although the harmonics are not as striking as that shown for the aquatic wave PSD of Figure 9, their positions correlate well with a model of the terrain consisting of varying degrees of order (shown by the blue curve). The low-frequency odd harmonics correspond to washboard-like swales on the order of 1.5 meters. These are odd-harmonics because they show a tendency to an asymmetric slant or tilt. The higher frequency even harmonics are caused by the Belgian block perturbations which are about 10 cm in lateral spacing.

The overall envelope suggests that a strong random walk component also exists, with a low density filter cutting off the high frequency sharpness in the terrain roughness. Over time, the cobblestones will wear down their sharp edges, and this is observed in the filtered trace.

The idea of using a superposition of various profiles from **Equation 7** makes sense since the various periodicities have very little mutual coherence, and the pair correlations are additive in contributing to the power spectrum.

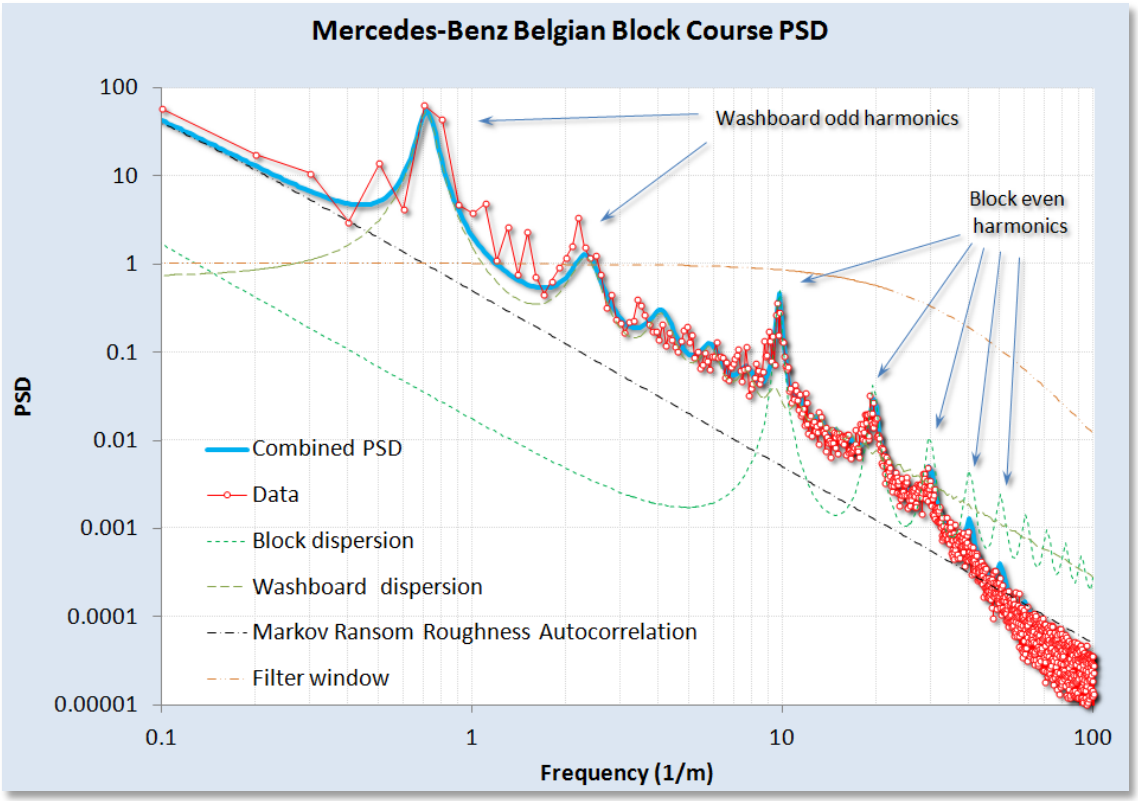


*Figure 18: A model fit to the Belgian Block course PSD. A rich variety of surface textures can be gleaned from the harmonics. At high wavenumbers, a change in slope is detected, likely due to a smoothing spatial filter applied to the fine terrain relief and partly due to interpolation for the OpenCRG data set*

For the Belgian block course, the data was not detrended prior to computing a spectrum. A slight tilt does exist in the data as can be gleaned from Figure 18, where several sections of 2D Fourier Transform PSD's for simulated (left and right) and real (center) terrains. The general approach of treating both the *Z* and *X* dimensions in a full power spectrum allows us to sensitively test for stepped or staircase surfaces.

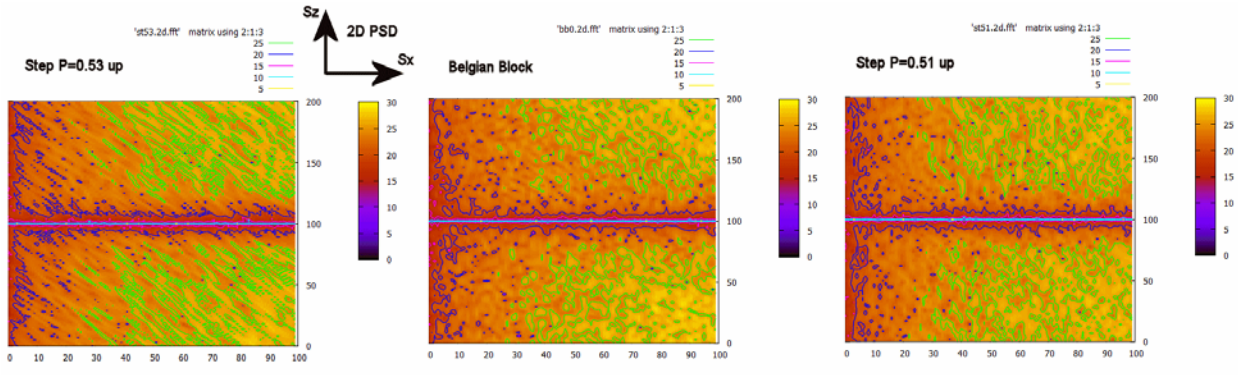


*Figure 19: Using the full 2D power spectrum, we can discern subtle changes in slope from any staircase pattern by looking at slanted texture. The center is the real data, and the two side maps show a slightly higher slope (left) and a slightly lower slope (right). The logarithm was taken of the PSD after the transform was multiplied by $S_x^2$ and $S_z^2$*

As a control study, we also collected PSD data from a military test course and compared the results in Figure 19. This data was detrended prior to use, with the PSD the only unclassified data available for analysis. Similar features are observed as with the Mercedes-Benz Belgian Block course, with the same washboard and block harmonics. These are slightly shifted in period likely due to different road construction and maintenance procedures.

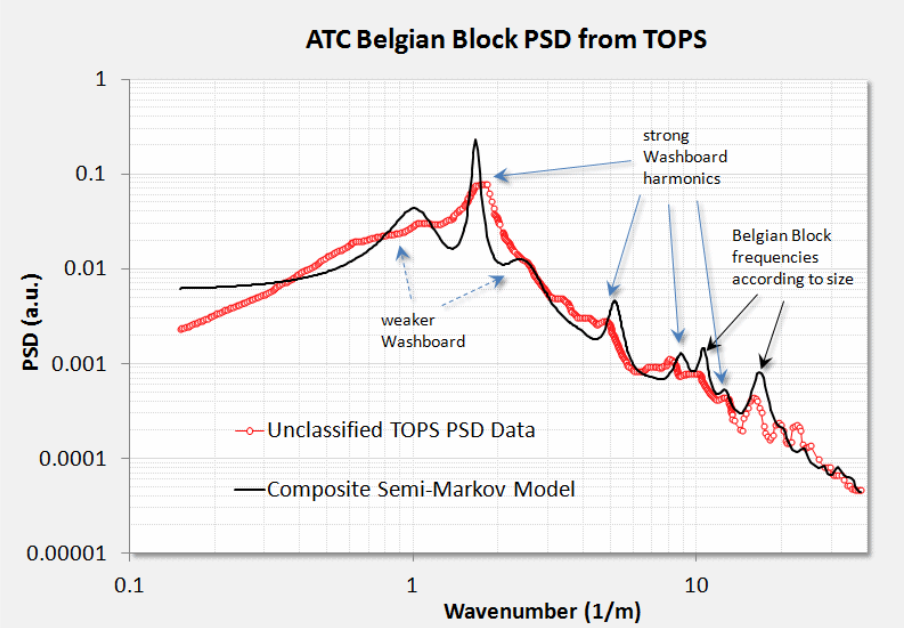


*Figure 20: Belgian Block course from a military test operational procedure (TOP) cocument.*

A few other profiles are worth considering. For Figure 20, from [30], we aligned an even-harmonic semi-Markov PSD with the empirically calculated PSD. The strong harmonics of a washboard road are expected as the repeated travel of vehicles over the course reinforces the washboard resonant frequency.

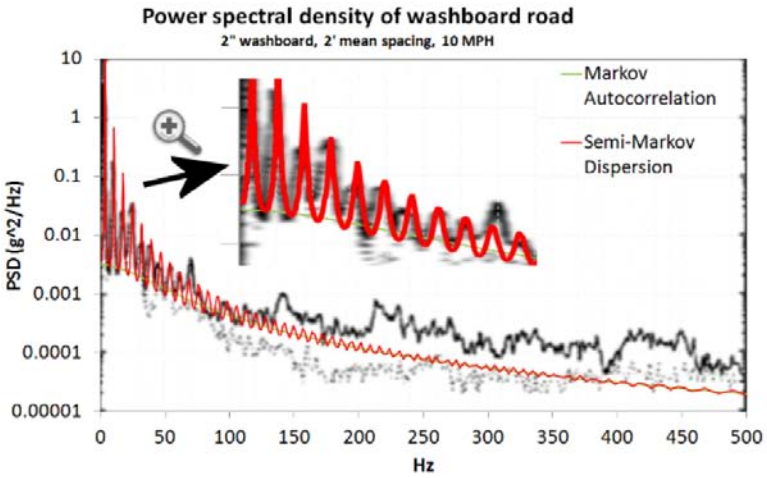


*Figure 21: A model fit to a pure washboard. The x-axis is expressed in Hz to indicate the test vehicle was maintaining travel at a constant speed.*

We can also return to the rough road power spectrum of Figure 4. We noted that this course likely contained a long-wavelength (deterministic) slope. The data was detrended as shown in Figure 21 below.

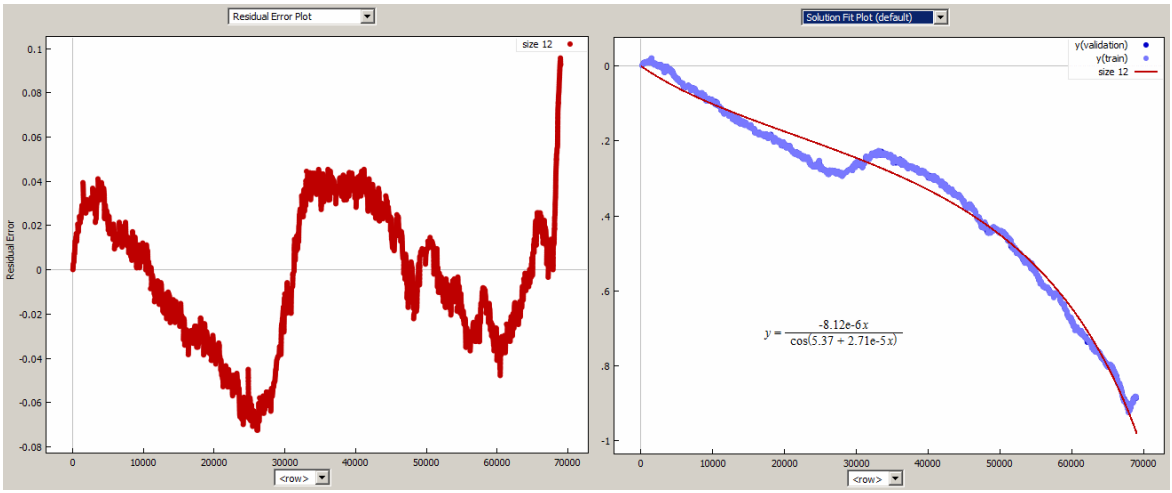


*Figure 22: The elevation trend in the rough road data set (right) was removed by a curve fitting program (**Eureqa**). The detrended residuals are shown to the left.*

After detrending the terrain profile, the rough-road PSD was calculated and fit to a semi-Markov model with one low-frequency component and a high-frequency periodic component as shown in Figure 22. The harmonics on the high-frequency spikes suggested that the underlying roughness was shaped. The first and second harmonics are strong, but the third roughly cancels out. By creating a two-level surface where the troughs were half as long as the tops, we could duplicate the missing third harmonic as shown by the solid red line in the figure.

A sinc function filter was added to reproduce the reduced strength of wavenumbers above 10/m.

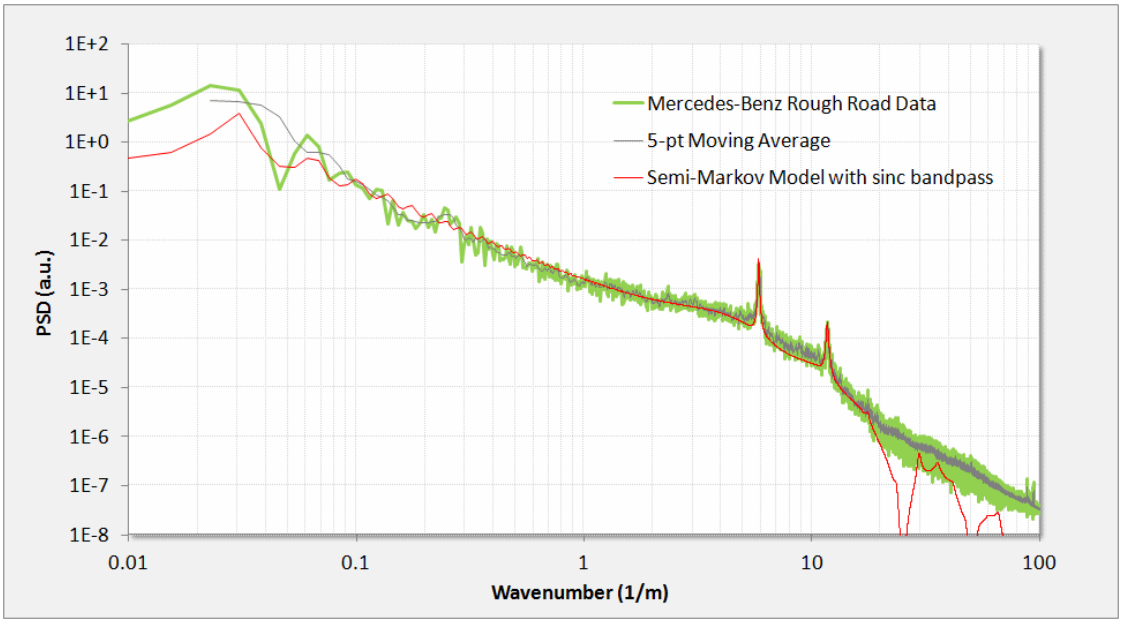


*Figure 23: Rough road PSD.*

The two-level spectra is a generalization of the result shown in **Equation 8**.

$$I_0(S_x, S_z) = \mathbb{Re}\left\{\frac{1}{S_x{}^2\langle L\rangle}\frac{\big(1-P(S_x)\big)(1-Q(S_x))}{1-P(S_x)Q(S_x)}\right\} \qquad \textbf{(9)}$$

Here each level has its own probability density of lengths, which allows for a surface with wider plateaus and narrower grooves.

$$P(S_x) = \frac{e^{-iS_xL_\alpha}}{1+{}^{iS_x}/_{\alpha}}, \qquad Q(S_x) = \frac{e^{-iS_xL_\beta}}{1+{}^{iS_x}/_{\beta}}$$

A simulated random walk for this terrain relief is shown in Figure 23 alongside an arbitrary path length from the actual terrain. To mimic the sinc filter, a rectangular window moving average was applied to the random walk profile. Note that after calibration of the relative step heights, very good qualitative agreement exists with the actual surface. (Full derivation in appendix)

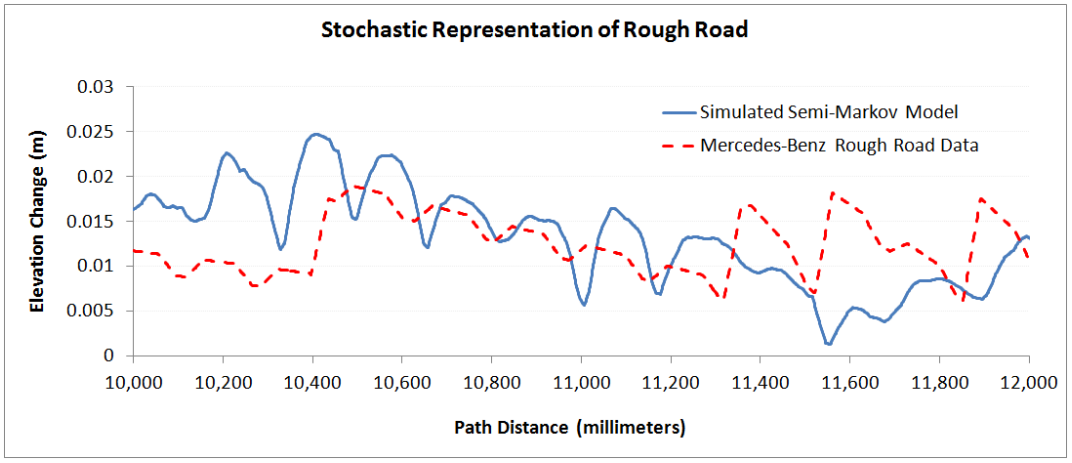


*Figure 24: Simulated random walk for the rough road terrain.*

As a check to determine whether we can recover the PSD from the simulated semi-Markov random walk, we applied a Fourier transform to 10 sets of simulation traces and squared the amplitude. Note the close alignment with the peaks and with the sinc filter poles. This demonstrates the general utility of switching between a stochastic analytical representation and a Monte Carlo generated simulation.

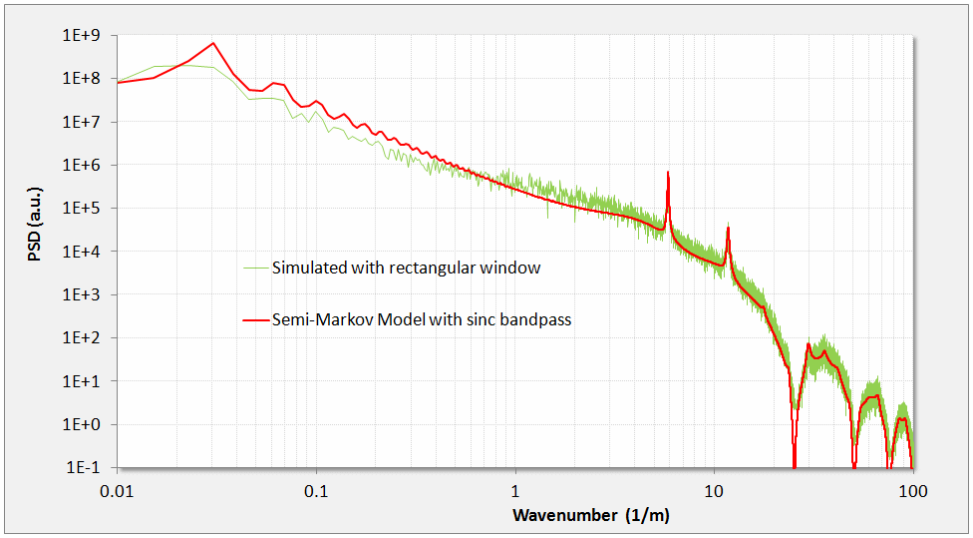


*Figure 25: A Monte Carlo simulation of the rough road semi-Markov behavior reveals nearly the same feature amplitudes for the assumed pair-correlation weightings.*

Finally, a varied test track featuring potholes and swale depressions[3] gives the PSD in Figure 25 showing relatively weaker periodicity.[31]

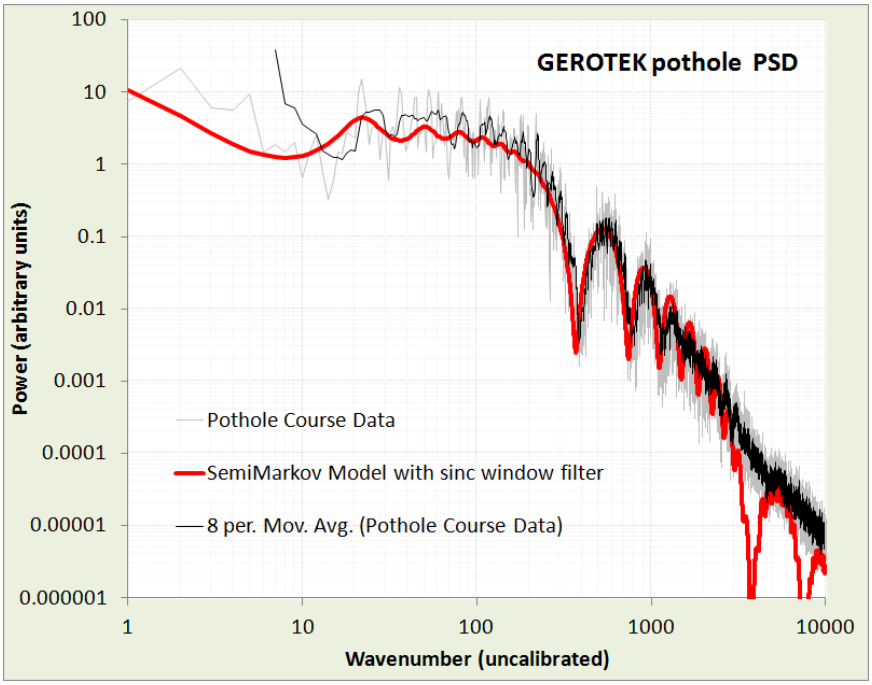


[3] This course is laid out in a loop of moderately irregular terrain. The native soil includes sassafras loam, a silty loam with 17.3-percent clay content, and sassafras silt loam with less than 15-percent clay. Surfaces range from smooth to rough, and there are sweeping turns. Under wet conditions, severe mud is present; when dry, the course is extremely dusty. Potholes and depressions are limited to 46-cm (18-in.) deep.

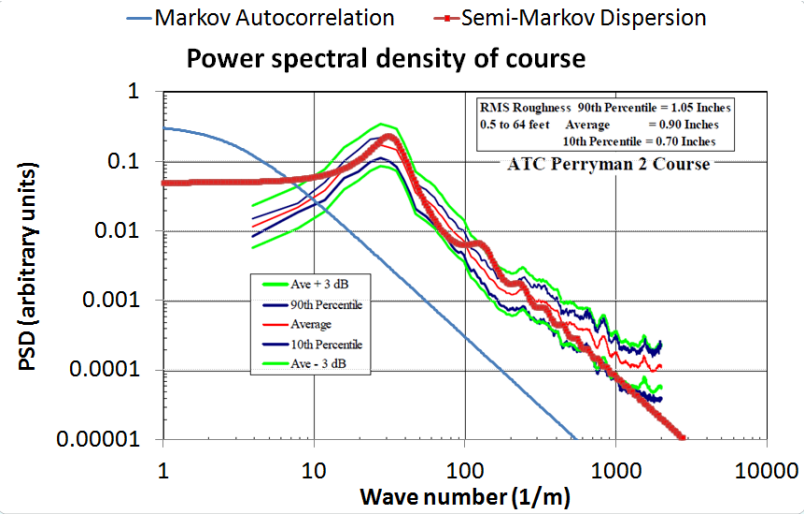


*Figure 26: Perryman 2 course*

# Generating Synthetic Terrains and Waves and Monte Carlo Sampling

Having a stochastic model of the terrain allows one to synthetically generate instances of the terrain that have the same spectral content. This becomes useful for mapping out an *ergodic* representation of possible terrain states suitable for *sampling* (i.e. *Monte Carlo*) simulations.

### Random Walk Model

The simplest *random walk* models generate the PSD corresponding to **Equation 4**, and exemplified by the empirical data in Figure 4 and simulated synthetic terrain in Figure 5. This is often referred to as *red noise* and it gives a fall-off as $1/S^2$.

As a typical algorithm for generating a Markov random walk in slope variations, assume $R$ is a sample from a uniform variate, $R \in [0..1]$.

A. Pick a slope from a sample PDF with mean θ
   Exponential : $\theta = -\alpha \ln(R)$
   Bessel : $\theta = \alpha \ln(R_1) \times \ln(R_2)$

B. Start at x=0 with that slope, θ

C. Let it propagate for a set run length x=L (cell size), this becomes a rise/run = θ′, if step size=1

D. Add a Markov random walk component that takes a random up or down slope of angle θ, for each cell length.
   if |R| < θ, then Δθ = θ sign(R-0.5) else stay on same level

E. This will create a random walk where < θ′> = θ for relatively small values of θ.

To better account for large slopes, the following algorithm generates the correct asymptotic trend for rise/run

```
if tan^-1(|R1|) < tan^-1 (θ) 2/π
then
   θ ln(R2)*sign(R3-0.5)+ elevation,
else
   stay on same level
```

The median slope tends to θ as the entire ergodic map is visited.

### Semi-Markov Process

The key to mapping to other semi Markov distributions is to draw from the appropriate PDF. For example, the delayed exponential (see **Equation 6**) is simply a draw from an exponential distribution with a fixed offset (i.e. the delay) added to the variate. The step deltas and terrace deltas can both draw from a semi-Markov distribution; taking the PSD of the resulting step sequence will generate a noisy **Equation 7**, depending on the amount of samples taken. The "rough road" data model generated in the previous section was specifically generated according to the recipe in the Appendix.

As an example of a simple semi-Markov model which will generate much of the spectral characteristics consider Figure 26 below and the Monte Carlo simulation which generates Figure 18. To illustrate a 2D power spectrum in terms of the orthogonal wavenumbers $S_x$ and $S_z$, we multiply by the wavenumber squared and then take the logarithm to give the greatest dynamic range. We first assume the simplest semi-Markov model, a damped exponential size for both step length and step height.

| | |
|---|---|
| log plot | $\mathrm{Re}\left(\left(1 - P - H \times \frac{(1-P)^2}{1 - H\,P}\right) z^2\right)$ where $P = \frac{1}{1 + i\,x}, H = \frac{1}{1 + i\,z}$ |

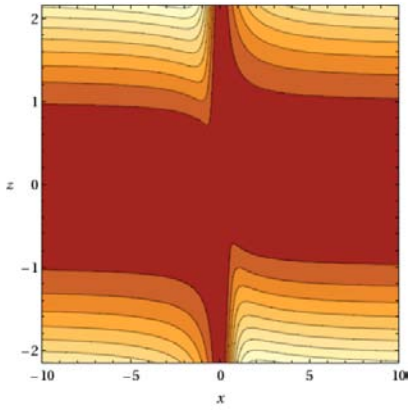


*Figure 27 : 2D contour plot of power spectrum for a randomly ascending staircase*

The algorithm for generating this semi-Markov model is as follows, where **P** is a probability of stepping up or down after each length. If **P** is not 0.5 precisely, then the two-dimensional PSD will show an asymmetry reflecting the asymmetry of the terrain profile.

```
BEGIN {
   N = 100000
   h = 0
   srand()
   i = N
   while(i>0) {
     n = - 10.0 * log(rand())
     for(j=0; j<n; j++) {
       i--
       print h
     }
     if(rand()>P) {
       h += +0.0008 * log(rand())
     } else {
       h += -0.0008 * log(rand())
     }
   }
}
```

The Belgian Block course suggests an asymmetry 0.51± 0.01 as shown in Figure 18, indicating sensitivity to incline.

### Ornstein-Uhlenbeck Process

The issue with a pure random walk model is that the absolute excursions become unbounded, whereas real data shows bounds in altitude in the terrain or waves. One way around this, which does not impact the spectral fall-off, is to attach a *reversion-to-the-mean* correction term to the random walk algorithm. This procedure is known as the *Ornstein-Uhlenbeck* random walk process[32], and derives from a physical model of an attractor or potential well which "tugs" on the random walker to bring it back to the mean state (see Figure 27 below).

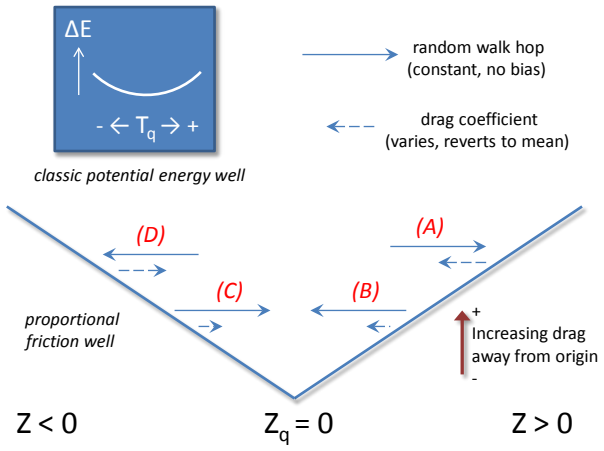


*Figure 28: Representation of an Ornstein-Uhlenbeck random walk process for terrain elevation changes. The hopping rate works similarly to a potential well, with a greater resistance to hopping the further excursion ways from a quiescent elevation ($Z_q$) changes.*

The following pseudo-code snippet sets up an Ornstein-Uhlenbeck random walk model with a reversion to the mean term. The *hop* term is the classical Markovian random walk transition rate. The *drag* term places an attractor which opposes large excursions in the terrain, *T*. Another term, *force*, generates a directional drift if the transition rate shows an asymmetry up versus down.

```
BEGIN {  ## Set up the Monte Carlo O-U model
   N = 300000
   hop = 0.02828
   drag = 0.005
   force = 0.0
   T[0] = 0.0

   srand()
   for(i=1; i<N; i++) {
     if(rand()<0.5) {
       T[i] = T[i-1] + (hop+force)*(1-T[i-1]*drag)
     } else {
       T[i] = T[i-1] - (hop-force)*(1+T[i-1]*drag)
     }
     print T[i]
   }
}
```

To determine whether an Ornstein-Uhlenbeck process is operational on a set of data, one can apply a simple multiscale variance (or a multiscale entropy measure[33]) to the result :

```
END {
   L = N/2;
   while(L > 1) {
     Sum = 0.0
     for(i=1; i<N/2; i++) {
        Val = T[i] - T[i+L]
        Sum += Val * Val
     }
     print L " " sqrt(Sum/(N/2))
     L = 0.95*L;
```

```
    }
}
```

So that for a given random walk simulation, the asymptotic variance will tend to saturate at longer correlation length scales. A typical multiscale variance plot will look like Figure 28. Even though this shows a saturation level, the power spectrum still obeys a $1/S^2$ fall-off.[34]

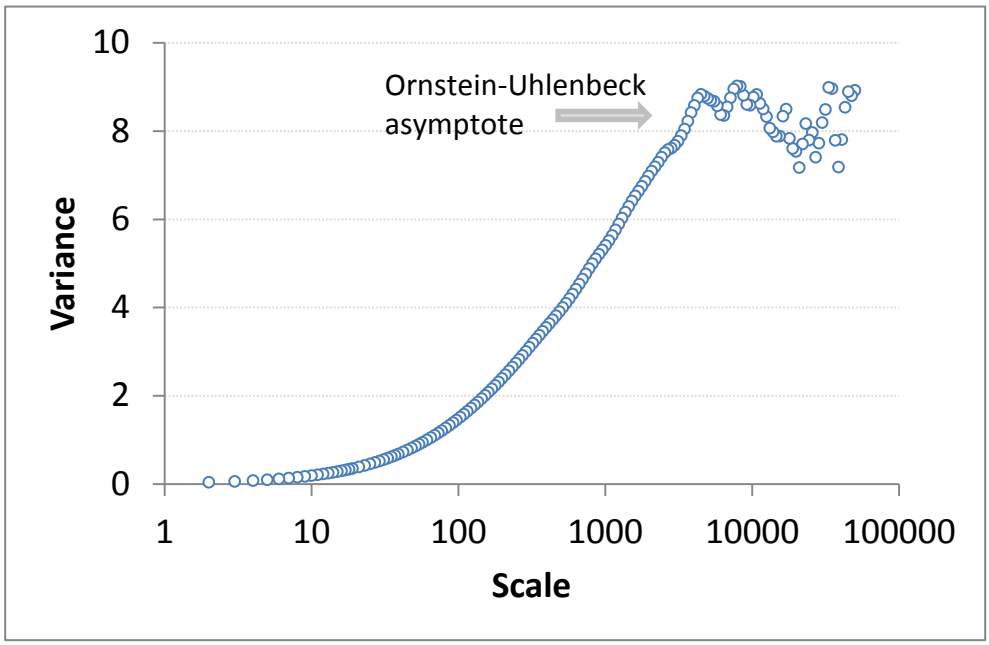


*Figure 29: Ornstein-Uhlenbeck process saturates on variance*

### Process Filters

If we wish to add a second-order Markovian feedback, we can filter the data with beyond near-neighbor interactions, i.e. not only **T[i]** and **T[i-1]** but **T[i-2]** and beyond. This adds an additional $1/S^2$ factor as it acts as a low-pass smoothing filter. In the case of an autocorrelation for a second-order step change:

$$c(x) = \int_{y=0}^{\infty} [\alpha^2 y\, e^{-\alpha y}] \cdot \left[\alpha^2 (y+x)\, e^{-\alpha(y+x)}\right] dy$$

This will generate a power spectrum of order 4:

$$I(S_x) = \frac{1}{\sqrt{2\pi}} \frac{\alpha^4}{(\alpha^2 + {S_x}^2)^2}$$

Ordinarily, we can apply the class of filters known as autoregressive models - AR($p$), where $p$ indicates the interaction order of the model, or in terms of digital processing, finite impulse response (FIR) filters. In general, these will all tend to smooth the simulation step changes, rounding out the edges as a low-pass filter is designed to work.

### Superposition of Waves

A non-stochastic method for generating a synthetic terrain involves extracting the Fourier coefficients from the PSD and superposing sine waves to recreate the original real-space terrain profile. This kind of inversion will generate a repeat sequence with multiples of the longest time period in the spectrum. No

phase information is available from the power spectrum, so any long range coherence is artificially introduced, unlike that from a pair correlation. Although potentially useful and practical [see our team member Ed Alexander's paper [35]], the superposition approach will definitely not traverse a complete state space and so is not ergodic. It will also not capture skewness and kurtosis in the terrain profile[36], of which the stochastic model can more easily (see Figure 24).

A good application of the spectral superposition approach is for generating aquatic waves for various sea-states in the incoherent regime.

### Sampling techniques

To make sampling efficient, particularly for rare events, techniques such as importance sampling[37] may be required. If a probability for a certain state is 10 orders of magnitude more rare than the most frequent state, the rule of thumb is that $10^{10}$ more samples may be required to catch this event. Importance sampling can cut the required number of samples down if the density function is well-characterized.

### Calibration of Spectra

The calibration of simulated terrains and their corresponding PSD curves to PSD calculations of actual terrains is aided by the application of Parseval's theorem[38]:

$$\langle z^2 \rangle = \int I(S) dS$$

This states that the statistical variance in the terrain elevation displacement is equivalent to the integrated power spectrum. In practice, as long as the variance in the real space sampling is stored, then the reciprocal space curve can be shifted by a constant scaling factor to match the variance.

## Discussion

Stochastic terrain modeling as described within this study finds practical application for vehicle test and verification applications,[39] with the terrain and energy models providing an environmental context for such activities as safety testing. We are essentially trying to map out the *Importance* × *Likelihood* space for the users of the context models. The users must know the impact or significance of the model effects as well as it likelihood of occurring.

The relevance for a particular topographical model depends on its intended usage. For example, one needs to ask the basic questions:

- What is the importance or impact of the event?
- What is the likelihood of the event?

These occupy largely orthogonal roles as shown in the figure below:


*Figure 30: Likelihood versus importance*

In the case of terrain, a vehicle operating over a rough profile would experience nuisance effects (vibration and absorbed power) that persistently occur. It could also potentially experience a critical effect (extreme slope) that rarely if ever occurs.

*Table 2: Orthogonal spaces*

| | Description | Examples |
|---|---|---|
| **High Likelihood** | Environmental stimulus that have high likelihood, but only a cumulative impact | Persistent and perpetual nuisance effects<br>▪ Terrain roughness and vibration<br>▪ Wear and tear<br>▪ Abrasion<br>▪ Wind friction and rolling resistance |
| **High Impact** | Environmental stimulus that have high impact but often low likelihoods | A critical effect that rarely if ever occurs<br>▪ A large shock<br>▪ Accidents<br>▪ 100-year climate events<br>▪ … lots of other possible cases<br>▪ … or some other pathological or unknown cases |

The overall goal is to provide models of environmental stimulus for design verification, using the probabilities inferred from the stochastic models to estimate correctness of the designs.

## Conclusion

A unified approach for characterizing and modeling topographies has definite advantages for environmental context applications. The extremely concise description presented demonstrates how often simple probability density functions (PDF) can characterize the impact/likelihood factors for various environmental behaviors. A stochastic basis for the models provides an explanation for empirically observed behavior that heuristics often miss. Further, unifying an established set of scientific and ontological criteria helps us to derive and classify the models.

# Appendix

## Creating Synthetic Terrain

1. Get terrain data [***x***, ***z***] as distance/displacement pairs
2. Run FFT on data assuming ***x*** equally spaced, and take magnitude squared
3. Fit the FFT curve to $w \cdot \mathrm{I}(s \mid \alpha, L)$
   $w$ = scaling
   $\alpha$ = local order
   $L$ = quasi-periodicity
   $s$ = wavenumber
$$\mathrm{I}(\mathrm{s} \mid \alpha, L) = \frac{1}{(\mathrm{s} - \alpha \cdot \sin(\mathrm{sL}))^2 + \alpha^2(1 + \cos(\mathrm{sL}))^2}$$
4. Draw a number of Monte Carlo samples from the PDF => $\mathrm{P}(x \mid \alpha, L)$.
   For each sample, use the cookbook inversion of a PDF to generate a step length, ***x***
$$\mathrm{x} = \mathrm{L} - \frac{1}{\alpha} \cdot \ln\big(\mathrm{rand}(\,)\big)$$
5. Move the step up and down alternately with amount corresponding to the RMS weighting of **w**
$$\mathrm{z} = \mathrm{c} \cdot \sqrt{\mathrm{L}}$$
   (if we need to detrend against large excursions, apply Ornstein-Uhlenbeck to ***z***)
6. Save the step lengths and step heights as a compact array of [***x***, ***z***] pairs
7. The intensity of a rough or cobbled terrain with differing lengths of troughs and tops is more complicated than that shown above. For the "rough road" model, we need to modify the step lengths to alternate depending on whether they lie on a trough or a top. The approach is straightforward but the pair correlation increases the number of terms in the intensity profile ( *I(s)* ) quadratically and so is not shown.

## Verifying the synthetic PSD

1. Get [***x***, ***z***] data from last terrain synthesis and discretize so that ***x*** is on equal intervals (for the FFT)
2. Run FFT and the magnitude squared
3. Compare the curves. Adjust the step size if magnitude is not to scale

## Two-level model

The resultant expression from **Equation (9)** is more complicated only because of the number of cross terms needed to pair correlate the two levels

$$\mathrm{I} = \frac{(\alpha S)^2 + (\beta S)^2 + (\alpha\beta)^2 S^4 - (\beta\, S)^2\, cos(SL_\alpha) - (\alpha\, S)^2\, cos\big(SL_\beta\big) + \alpha\beta^2 S^3 \sin(SL_\alpha) + \alpha^2 \beta S^3 \sin(SL_\beta)}{\big(1 - \alpha\beta S^2 - \cos\big(S(L_\alpha + L_\beta)\big)\big)^2 + (\alpha S + \beta S + \sin\big(S(L_\alpha + L_\beta)\big))^2}$$

To generate a synthetic terrain, each level is treated as a sampling distribution with respective parameters.
(as)^2+(bs)^2+(as)^2*(bs*s)^2 -cos(la*s)*(bs)^2-cos(lb*s)*(as)^2+sin(la*s)*(bs)^2*as*s+sin(lb*s)*(as)^2*bs*s) /

((-(s*a)*(s*b)-cos((s*la)+(s*lb))+1)^2+((s*a)+(s*b)+sin((s*la)+(s*lb)))^2)

Extra

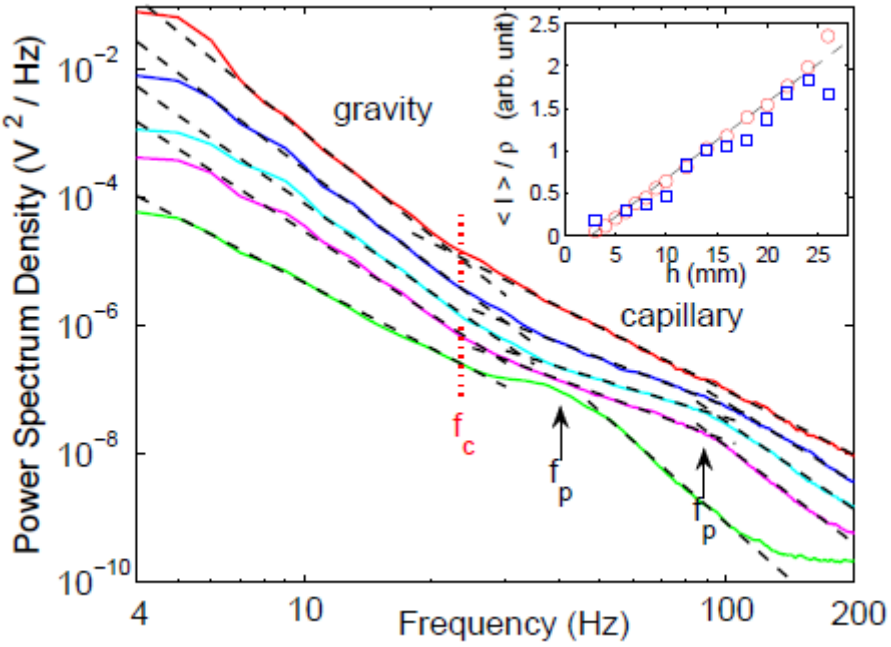


*Figure 31 : Power law fall-off* [40]

# References

[1] M. Waechter et al., "Stochastic Analysis of Surface Roughness -," *EPL (Europhysics Letters)* 64, no. 5 (2003): 579.
[2] R. H Stewart, *Introduction to Physical Oceanography* (A & M University, 2003), http://kingfish.coastal.edu/physics/msci301/stewart/TOC.pdf.
[3] A. Leon-Garcia, *Probability, Statistics, and Random Processes for Electrical Engineering* (Prentice Hall, 1994).
[4] D. Mumford and A. Desolneux, *Pattern Theory: The Stochastic Analysis Of Real-World Signals* (A K Peters, Ltd., 2010), http://www.dam.brown.edu/ptg/MDbook/index.html.
[5] P. R. Pukite and J. Pukite, "Digital Signal Processors for Computation Intensive Statistics and Simulation," *SIGSIM Simul. Dig.* 21, no. 2 (December 1990): 20–29.
[6] P.R. Pukite, *The Oil Conundrum: Vol. 1 Decline, Vol. 2 Renewal*, vol. 1,2, 2 vols. (Daina, 2011), http://books.google.com/books/about/The_Oil_Conundrum.html?id=oY2ZPn5EOTQC.
[7] K. Chowdary, "Distinguising and Integrating Aleatoric and Epistemic Variation in UQ" (Brown University, 2011), http://www.dam.brown.edu/documents/Chowdhary.pdf.
[8] E.T. Jaynes and G.L. Bretthorst, *Probability Theory: The Logic of Science* (Cambridge Univ Pr, 2003).
[9] C. Beck, "Generalized Statistical Mechanics for Superstatistical Systems," *Philosophical Transactions of the Royal Society A: Mathematical, Physical and Engineering Sciences* 369, no. 1935 (December 13, 2010): 453–465.
[10] P. Pukite and S. Bankes, "Entropic Complexity Measured in Context Switching," in *Applications of Digital Siignal Processing*, vol. 17 (InTech, 2011), http://www.intechopen.com/books/applications-of-digital-signal-processing/entropic-complexity-measured-in-context-switching.
[11] P.R. Pukite and J. Pukite, *Markov Modeling for Reliability Analysis* (Wiley-IEEE Press, 1998).
[12] P. R. Pukite, C. S. Lent, and P. I. Cohen, "Diffraction from Stepped Surfaces:: II. Arbitrary Terrace Distributions," *Surface Science* 161, no. 1 (1985): 39–68.
[13] Ibid.
[14] "OpenCRG Homepage", n.d., http://www.opencrg.org/.
[15] P.R. Pukite, *Reflection High Energy Electron Diffraction Studies of Interface Formation* (University of Minnesota, 1988), http://books.google.com/books?id=QbKN59MGbrUC.
[16] PATRICK HOLMES, PhD, "A COURSE IN COASTAL DEFENSE SYSTEMS I CHAPTER 5 COASTAL PROCESSES: WAVES," *CDCM Professional Training Programme, 2001*, n.d., http://www.oas.org/cdcm_train/courses/course21/chap_05.pdf.
[17] Stewart, *Introduction to Physical Oceanography*.
[18] Ibid.
[19] Huang, T.; Alarcon, C.; Bingham, A.; Henderson, M. L.; Kessling, M.; Takagi, A.; Thompson, C. K, "NASA ADS: Data-Driven Oceanographic Web Portal", n.d., http://adsabs.harvard.edu/abs/2010AGUFMIN23A1350H.
[20] "CDIP Homepage", n.d., http://cdip.ucsd.edu/?units=metric&tz=UTC&pub=public&map_stati=1,2,3.
[21] T. S. Rhee et al., "Influence of Energetic Wind and Waves on Gas Transfer in a Large Wind–wave Tunnel Facility," *J. Geophys. Res.* 112, no. C5 (May 16, 2007): C05027.
[22] F. Feddersen and F. Veron, "Wind Effects on Shoaling Wave Shape," *Journal of Physical Oceanography* 35, no. 7 (2005): 1223–1228.
[23] William B. Wright et al., "Imaging of Intermittency in Ripple-Wave Turbulence," *Science* 278, no. 5343 (November 28, 1997): 1609 –1612.
[24] DZ Ning et al., "Free-surface Evolution and Wave Kinematics for Nonlinear Uni-directional Focused Wave Groups," *Ocean Engineering* 36, no. 15 (2009): 1226–1243.
[25] Pukite, *The Oil Conundrum: Vol. 1 Decline, Vol. 2 Renewal*, 1,2:.
[26] "BTRC Track Features", n.d., http://www.vss.psu.edu/BTRC/btrc_track_features.htm.
[27] E.E. Fitch, "Durability Analysis Method for Nontationary Random Vibration" (MIT, 1996), http://dspace.mit.edu/bitstream/handle/1721.1/40004/35651567.pdf.
[28] Automotive Directorate, "1-1-010 Vehicle Test Course Severity (Surface Roughness)", 2006, file:///T:/prog/shared/modsim/public_html/context/svn/trunk/Ontology/library/reference/1-1-010%20Vehicle%20Test%20Course%20Severity%20(Surface%20Roughness.pdf.
[29] "OpenCRG Homepage."
[30] G.F. Sievert, "Effects of Stabilizer Bars on Road Vehicle Ride Quality" (Rice, 1994), zotero://attachment/111/.

[31] Automotive Directorate, "1-1-010 Vehicle Test Course Severity (Surface Roughness)."
[32] Mumford and Desolneux, *Pattern Theory: The Stochastic Analysis Of Real-World Signals*.
[33] Pukite and Bankes, "Entropic Complexity Measured in Context Switching."
[34] B. Lindner, "A Brief Introduction to Some Simple Stochastic Processes," *Stochastic Methods in Neuroscience* (2009): 1.
[35] J.E. Alexander, "Synthesis of a PSD Compatible Acceleration Time-History," *Submitted to Shock & Vibration Symposium (November 5-9, 2012)* (n.d.).
[36] A. Steinwoff and W.H. Connon III, "Limitations of the Fourier Transform for Describing Test Course Profiles," *Sound and Vibration* 39, no. 2 (2005): 12–17.
[37] M. Denny, "Introduction to Importance Sampling in Rare-event Simulations," *European Journal of Physics* 22 (2001): 403.
[38] L. Romero and W.K. Melville, "Spatial Statistics of the Sea Surface in Fetch-Limited Conditions," *Journal of Physical Oceanography* (2011).
[39] Jonathan Cameron et al., *Vehicle-Terrain Interaction Modeling and Validation for Planetary Rovers* (Dartslab: NASA JPL, 2009), http://trs-new.jpl.nasa.gov/dspace/bitstream/2014/41675/3/10-15.pdf.

[40] E. Falcon and C. Laroche, "Observation of Depth-induced Properties in Wave Turbulence on the Surface of a Fluid," *EPL (Europhysics Letters)* 95 (2011): 34003.